SAND REPORT
SAND2002-3538
Unlimited Release
Printed December 2002

Material Characterization of Glass, Carbon, and Hybrid-Fiber SCRIMP Panels

Akira Kuraishi, Stephen W. Tsai, and Julie Wang
Stanford University
Department of Aeronautics and Astronautics
Stanford, California

Prepared by
Sandia National Laboratories
Albuquerque, New Mexico 87185 and Livermore, California 94550

Sandia is a multiprogram laboratory operated by Sandia Corporation, a Lockheed Martin Company, for the United States Department of Energy's National Nuclear Security Administration under Contract DE-AC04-94-AL85000.

Sandia National Laboratories

Issued by Sandia National Laboratories, operated for the United States Department of Energy by Sandia Corporation.

Available to DOE and DOE contractors from
U.S. Department of Energy
Office of Scientific and Technical Information
P.O. Box 62
Oak Ridge, TN 37831

Telephone: (865)576-8401
Facsimile: (865)576-5728
E-Mail: reports@adonis.osti.gov
Online ordering: http://www.doe.gov/bridge

Available to the public from
U.S. Department of Commerce
National Technical Information Service
5285 Port Royal Rd
Springfield, VA 22161

Telephone: (800)553-6847
Facsimile: (703)605-6900
E-Mail: orders@ntis.fedworld.gov
Online order: http://www.ntis.gov/help/ordermethods.asp?loc=7-4-0#online

SAND2002-3538
Unlimited Release
Printed December 2002

Material Characterization of Glass, Carbon, and Hybrid-Fiber SCRIMP Panels

Akira Kuraishi, Stephen W. Tsai, and Julie Wang
Stanford University
Department of Aeronautics and Astronautics
Stanford, California

Abstract

The purpose of this study was to generate the material database for carbon and glass composite panels created by the SCRIMP process. The materials tested were glass/polyester composites, two types of carbon/polyester composites, and carbon and glass hybrid composites. The differences between the two types of carbon/polyester, which we call Type 1 and Type 2, are the ply thickness (.037"/ply and .048"/ply) and slightly different treatment of polyester resin. The tests that were performed for this study are four-point-bending tests, tension tests, panel warping tests, and beam bend-twist coupling tests. The material properties of interest were basic longitudinal and transverse stiffness and strength, residual stress due to curing, and the effect of bend-twist coupling. The bend-twist coupling is a feature that can be added to the composite laminate or structure, such that when it is bent, it will also twist.

Sandia Technical Monitors:

Paul Veers
Tom Ashwill

This is a Contractor Report for Sandia National Laboratories that fulfills the deliverables under Contract #22163.

Introduction

SCRIMP is a low-cost, large-scale manufacturing process of composite materials that has been used for various applications from boats, trains, buses, and wind turbine blades. This is a patented process of TPI Composites, Warren, RI. The intended application of this database is the design of carbon and glass hybrid composite wind turbine blades.

Currently post-curing is not performed in SCRIMP, which may or may not lead to increased performance. The effects of post-cure on the stiffness and strength were studied in this report using typical coupon test and panel warping tests.

Another effect studied was the bend-twist coupling of the hybrid laminate. The bend-twist coupling is a feature that can be added to the composite laminate or structure, such that when it is bent, it will also twist. This feature can be used as the passive control of the blade pitch.

1. Bending Tests

The purpose of the bending tests was to evaluate the basic material properties at both virgin and post-cured conditions. The post-cure is known to affect both the stiffness and the strength for the material systems that are not fully cured. The tested material systems were all room temperature cured, and thus certain effects of post-cure were expected.

1.1 Test Configuration

The four-point-bending tests were performed on three material systems, namely the glass/polyester composite, and two types of carbon/polyester composites. The differences between the two types of carbon/polyester, which we call Type 1 and Type 2, are the ply thickness (.037"/ply and .048"/ply) and slightly different treatment of polyester resin.

The virgin materials were impregnated with polyester resin using the SCRIMP process and room temperature cured. The post-cure was performed in two different configurations. In one case, the post cure temperature was gradually increased up until 100°C, and in the other case kept constant at 60°C. 60°C was chosen since it is possible to heat large structures up to this temperature without using an oven or an autoclave.

The tests were performed in both the longitudinal and transverse directions. Figure 1 shows the test configuration of the four-point-bending tests.

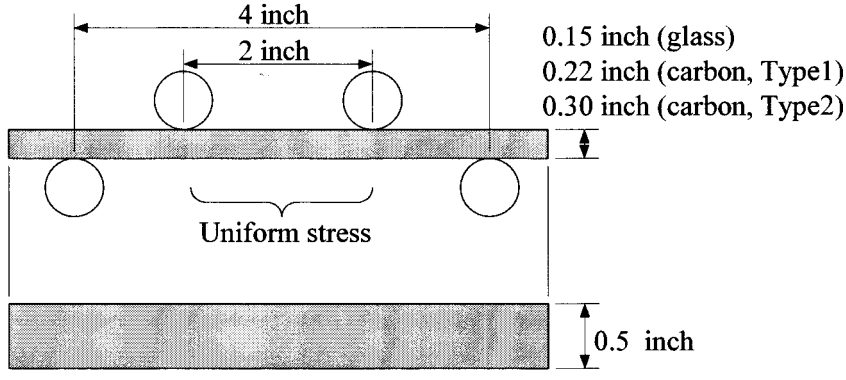

Figure 1 4 point bending test configuration

The flexural moduli were obtained from the initial slope of the stress-strain curve, and the strengths were calculated from the maximum stresses at failure. The measurable strength for each material and test configuration is determined by the failure modes and is summarized in Table 1.

Table 1 Failure modes and measured strength

Material	Configuration	Failure mode	Measured strength
Glass/Polyester	Longitudinal Transverse	Compression Tension	Longitudinal compression X' Transverse tension Y
Carbon/Polyester	Longitudinal Transverse	Inter-laminar shear Tension	Shear S Transverse tension Y

1.2 Test Results

Table 2 shows the test results of the four-point-bending tests of three types of materials. The moduli were calculated by ignoring the effect of the shear deformation, which can be significant for a thick specimen with relatively low shear modulus. This was the case for the Type 2 carbon/polyester composites. E_x and E_y are the longitudinal and transverse moduli, respectively. X, X', Y, Y', and S are the longitudinal tensile, longitudinal compressive, transverse tensile, transverse compressive, and shear strengths, respectively. (See Appendix A for detailed test results.)

Table 2 Bending test measurements

Material	Items		Virgin material		Post-cured material*[1]		
			measurement	specimens	measurement	specimens	change
E-glass/polyester	*Ex*	(msi)	5.62	4	5.58	3	-1%
	Ey	(msi)	1.15	5	1.39	3	21%
	X'	(ksi)	86.3	4	89.5	3	4%
	Y	(ksi)	3.16	5	3.36	3	6%
	S	(ksi)	>3.25	4	>3.36	3	
Carbon/polyester (Type 1)	*Ex*	(msi)	10.5	1	11.4	1	*2
	Ey	(msi)	0.75	3	0.88	3	17%
	X	(ksi)	>92.6	1	>106	1	
	Y	(ksi)	4.29	3	3.90	3	-9%
	S	(ksi)	5.14	1	5.81	1	*2
Carbon/polyester (Type 2)	*Ex*	(msi)	8.61	5			
	Ey	(msi)	0.76	5			
	X	(ksi)	>44.1	5			
	Y	(ksi)	4.24	5			
	S	(ksi)	3.29	5			

*1 Post-cure was performed at 60°C for 8 hours.
*2 Insufficient numbers of specimens

1.3 Effect of the Post-Cure

The most significant effect of the post-cure was on the transverse modulus, which increased about 20% after 8 hours of exposure at 60°C for both material systems. For the glass/polyester composites, small increases in the longitudinal compression and transverse tension strengths were observed, but no clear increase in the longitudinal modulus was observed. For carbon/polyester composites, the number of specimens was insufficient to reach a conclusion of the effect of the post-cure.

We have also observed that the post-cure has an effect on the residual stress, which is summarized later in Section 5.4. The conclusion is that the post-cure will increase the residual stress in a laminate with plies in two or more directions.

Performing a post-cure will inevitably lead to increased manufacturing cost. Whether the observed changes in the performance can justify this cost increase will depend on each application. Therefore, we will not attempt to conclude whether the post-cure is necessary or not.

2. Tension Tests

The purpose of the tension tests was to obtain more information on the basic material properties of the Type 2 carbon/polyester composites. The material properties measured from the tension tests and bending tests are known to be different, which was the case in this material also.

2.1 Test Configuration

The tension tests were performed on the Type 2 carbon/polyester composites in both the longitudinal and transverse directions. The test specimens for both tests are shown in Figure 2. The test specimen was attached to the test machine using the hydraulic grips on both ends, which were reinforced with the bonded GFRP tabs.

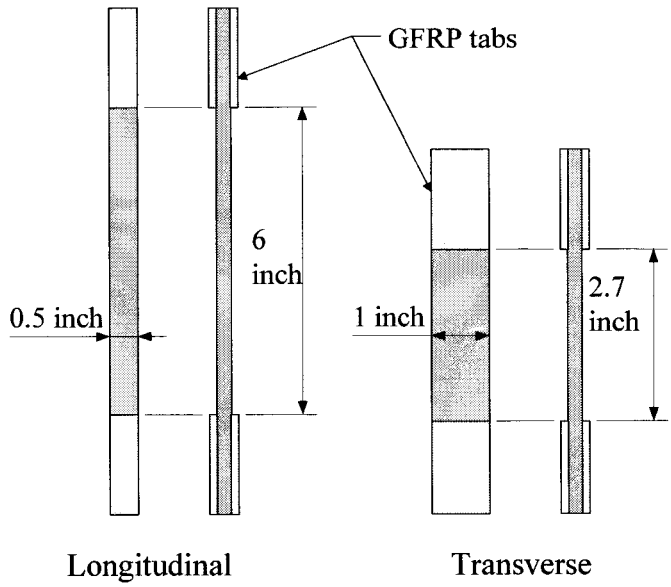

Figure 2 Tension test specimens

The strain was measured using the extensometer, and the stress was calculated from the applied load divided by the cross section area. The longitudinal and transverse moduli were obtained from the initial slope of the stress-strain curve, and the strengths were calculated from the maximum stresses at failure. Unfortunately, the longitudinal tensile strength X could not be measured since all the longitudinal test specimens failed prematurely at the tab due to the out-of-plane compression force from the hydraulic grip. The transverse test specimens failed in tension, and therefore the transverse tensile strengths Y could be measured.

2.2 Test Results

Table 3 shows the results of the tension tests of the Type 2 carbon/polyester composites. (See Appendix A for detailed test results.)

Table 3 Tension test measurements

Material	Items		Virgin material	
			measurement	specimens
Carbon/polyester	*Ex*	(msi)	12.6	5
(Type 2)	*Ey*	(msi)	0.92	6
	X	(ksi)	N/A	
	Y	(ksi)	1.76	6
	S	(ksi)	N/A	

2.3 Comparison

The tension tests are considered to be more accurate than the bending tests in measuring the modulus and the strength. Compared to the tension tests, the results from the bending tests showed lower modulus and higher transverse tensile strength. It is common to have lower modulus measurements from the bending tests, which is called the "flexural modulus". The lower modulus may be attributed to the shear deflection of the specimen and the local deflection at the load points, both ignored in the calculation.

The difference in the measured transverse tensile strengths can be related to the initial flaws in the test specimens. In tension tests, the specimen will fail from the weakest link, which can be located anywhere in the specimen. In four-point-bending tests, the region of high stress is limited to the lower surface between the two loading points. If the flaws were randomly located, the strength measurements from the tension tests are more likely to be lower. By the same reason, the strength of a three-point-bending test data should be the highest having a line load where the failure occurs, as compared with a surface or body failure sites for the four-point-bending and tension tests, respectively.

3. Warping Tests

The purpose of the warping test was to determine the residual stress due to cure and to estimate the thermal coefficient of expansion of the material. The tests were performed on the glass/polyester composite and two types of carbon/polyester composites.

3.1 Test Configuration

The panel specimens were intentionally manufactured in an asymmetric layup, $[0_3/90_3]$. When cured, the difference in the contractions in longitudinal and transverse directions creates significant residual stresses. If the panel is not constrained, these stresses will warp the panel into either the anticlastic shape (also known as "saddle shape") shown in Figure 3, or the cylindrical shape depending on the dimension of the panel.

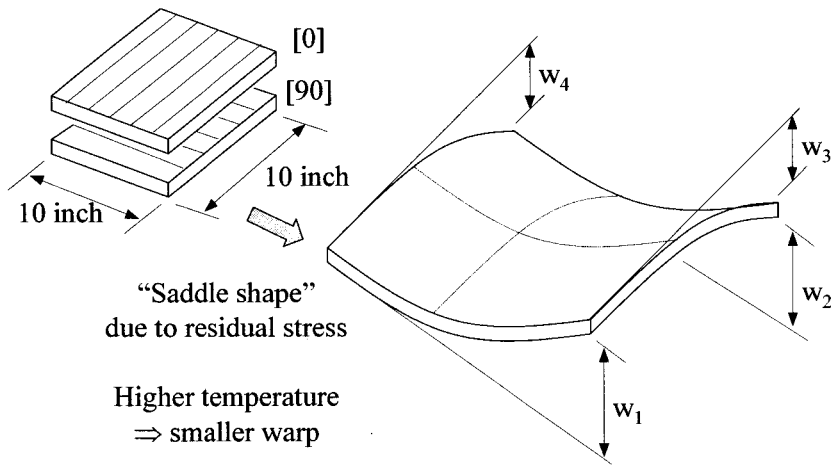

Figure 3 Warping test configuration

Commonly, this residual stress is attributed to the curing temperature of the composites, and therefore no residual stress was expected for the panel cured at room temperature. To our surprise, we observed significant warp on the room-temperature-cured panels, indicating the presence of significant residual stress. We suspect two sources of shrinkage that lead to this residual stress. One is the natural shrinkage of the resin during the cure process, which is independent of the curing temperature. Another source is the thermal expansion due to the elevated temperature caused by the exothermal condition during the cure, which is common in typical epoxy and polyester resins. In other words, although no additional heat was added, the resin heated up during the cure process and hardened at this elevated temperature. When the panel cooled down to room temperature, the resin contracted and contributed partly to the residual stress.

The warp can be minimized or eliminated by using the symmetric layup instead of the asymmetric layup, but this will not reduce the residual stress. In fact, the plies are forced to be flat, which leads to significantly larger residual stress.

3.2 Test Results

Table 4 shows the test results for the first type of warp test that was performed to observe the effect of post-cure on the residual stresses. The value of the warp is the average of the eight measurements for each condition. The residual stress at flat condition is calculated using the following equation.

$$\sigma_R = \frac{8}{t^2 L^2 (d_{11} - d_{12})} w \qquad (1)$$

where t is the thickness, L is the length and the width of the panel, w is the average value of the warp at the corner. d_{11} and d_{12} are the components of the flexural compliance matrix [d], with a unit of [1/lbf-in] or [1/psi-in^3]. (See Appendix B for more details.)

In addition to the post-cure, the panels were soaked in 60°C water for 100 hours to observe the change in residual stress at saturated condition. The moisture is known to expand the material and compensate for the thermal shrinkage. The effect was observed, but to a smaller degree than expected. The carbon panel showed smaller moisture absorption compared to the glass panel, and thus less reduction in the residual stress.

Table 4 Warp test measurements (Post-Cure Effect)

Specimen	Conditioning	Measured at	Warp (in)	Warp (relative)	Residual stress* (ksi)	Note
Glass Panel 1	none	RT, Dry	0.30	1.0	0.6	
	60Cx.5hrs	RT, Dry	0.43	1.5	0.9	
	+ 80Cx.5hrs	RT, Dry	0.59	2.0	1.2	
	+ 80Cx.5hrs	RT, Dry	0.78	2.6	1.6	
	+ 100Cx.5hrs	RT, Dry	0.81	2.7	1.7	
Glass Panel 2	none	RT, Dry	0.33	1.0	0.7	
	60Cx4hrs	RT, Dry	0.57	1.7	1.2	
	60Cx8hrs	RT, Dry	0.64	1.9	1.3	
	Soak 60Cx100hrs	RT, Wet	0.49	1.5	1.0	weight gain of 2.5%
Carbon (Type1) Panel 2	none	RT, Dry	0.15	1.0	0.5	
	60Cx4hrs	RT, Dry	0.33	2.1	1.2	
	60Cx8hrs	RT, Dry	0.40	2.6	1.4	
	Soak 60Cx100hrs	RT, Wet	0.36	2.3	1.2	weight gain of 0.28%

* The residual stress is calculated at the flat condition

Figure 4 shows the change in the residual stress of the glass and carbon composite panels after several steps of post-cure at 60°C. We observe that the residual stresses in carbon and glass panels are similar. Typically, glass composites have less residual stress since the glass fibers also expand with temperature, while carbon fibers are known to show very small expansion or even shrinkage at elevated temperature.

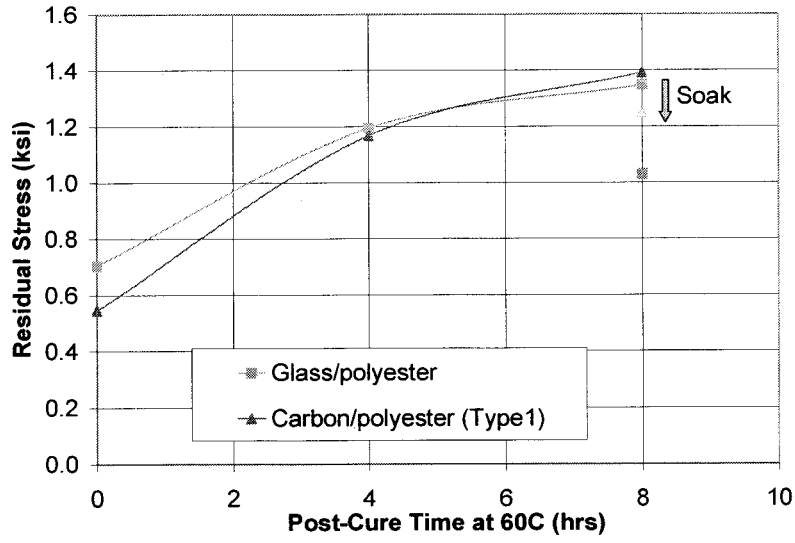

Figure 4 Effect of post cure on the residual stress

Table 5 shows the second type of warp test, where we attempt to measure the coefficient of thermal expansion (CTE). This can be done by measuring the warp at elevated temperature and comparing the value with the original warp at room temperature. This test was complicated by two problems. The first problem was that each time the temperature was increased the effect of post-cure increased the warp and therefore changed the baseline. Another problem was that since the panel cooled down quickly during the measurements, only the first few measurements were accurate. In order to solve these problems, the room temperature measurements after each post-cure was used as the baseline of comparison, and only the first measurements at each condition were used. We can observe that the measured values of warp per elevated temperature are almost constant. The CTEs can be calculated from these values, which will be shown in the next section.

Table 5 Warp test measurements (High temperature)

Specimen	Conditioning	Measurement 1		Measurement 2		Difference	
		Temp (C)	Warp (in)	Temp (C)	Warp (in)	ΔT (C)	Warp/ΔT (in/C)
Glass Panel 1	none	23	0.32				
	60Cx.5hrs	23	0.46	60	0.27	37	-0.0054
	+80Cx.5hr	23	0.57	80	0.17	57	-0.0069
	+80Cx.5hr	23	0.82	80	0.47	57	-0.0061
	+100Cx.5hrs	23	0.83	100	0.31	77	-0.0068

Table 6 shows the third type of warp test, in which the material is cooled down rather than heated. As mentioned above, heating up the panel effectively post-cures it and affects the warp measurement. No post-cure effect from cooling the panel is expected, and thus the baseline value of the warp should not change. The panel was cooled in the freezer to achieve −14°C, and dry ice was used to achieve −78°C. Only the first two measurements were used for each condition for the same reason as before.

Table 6 Warp test measurements (Low temperature)

Specimen	Conditioning	Measured Temp (C)	Warp (in)	Warp (relative)	Warp/ΔT (in/C)	Residual stress* (ksi)
Glass	none	23	0.48	1.0		1.0
Panel 3	none	-14	0.69	1.4	-0.0057	1.4
	none	-78	0.87	1.8	-0.0039	1.8
Glass	none	23	0.44	1.0		0.9
Panel 4	none	-14	N/A			
	none	-78	0.84	1.9	-0.0040	1.8
Carbon (Type2)	none	23	0.21	1.0		1.2
Panel 1	none	-14	0.40	1.9	-0.0051	2.2
	none	-78	0.49	2.3	-0.0028	2.7
Carbon (Type2)	none	23	0.21	1.0		1.2
Panel 2	none	-14	N/A			
	none	-78	0.52	2.5	-0.0031	2.9

* The residual stress is calculated at the flat condition

The measured warp per change in temperature of the glass panel at −14°C is similar to the value observed in the previous test shown in Table 5. The CTEs are known to change with temperature, which is presumably why the warp per change in temperature is lower at −78°C.

It is interesting to note that cracks were observed in the glass panels after they were cooled down to −78°C. The residual stress is reduced but still exists at the warped condition, which will be calculated in the next section. (See Appendix A for detailed test results.)

3.3 Analysis

Warping of the asymmetric laminate can be calculated by the lamination theory as shown in Appendix B. In this section, we will use the derived equation to calculate the coefficient of thermal expansion (CTE) and the stress free temperature.

The residual stress in the flat condition can be calculated from the CTEs in the longitudinal and transverse directions, α_x and α_y, respectively.

$$\sigma_R = \frac{Q_{xx}Q_{yy} - Q_{xy}^2}{Q_{xx} + 2Q_{xy} + Q_{yy}}(\alpha_y - \alpha_x)\Delta T \tag{2}$$

By combining Equations (1) and (2),

$$(\alpha_y - \alpha_x) = \frac{Q_{xx} + 2Q_{xy} + Q_{yy}}{Q_{xx}Q_{yy} - Q_{xy}^2} \frac{8}{t^2 L^2 (d_{11} - d_{12})\Delta T} w \tag{3}$$

where Q_{ij} are components of the stiffness matrix [Q] of the unidirectional lamina.

Note that we can only calculate the difference between the two CTEs. Calculating the individual values of the CTE requires precision measurements of the expansion in the longitudinal and transverse directions. Instead, we will use the longitudinal CTE α_x taken from a textbook [1].

Another important value that can be calculated from these results is the stress-free temperature. This is the temperature were the residual stress becomes zero, which is related to the curing temperature. This value can be measured experimentally by observing the temperature in which the warped panel becomes flat, or by using the following equation.

$$T_{\sigma\, free} = T_{RT} - \frac{w_{RT}}{w/\Delta T} \tag{4}$$

where T_{RT} is the room temperature and w_{RT} is the measured warp at this temperature.

The calculated values of CTEs and the stress free temperature for the glass/polyester and Type2 carbon/polyester are summarized in Table 7. In this calculation, material properties from the bending tests were used for the glass composites. For Type 2 carbon composites, material properties from the tension tests were used since they are considered to be more accurate.

Table 7 Coefficients of thermal expansion and stress-free temperature

Material	Warp per temp $w/\Delta T$	CTE [e-6/C]			Stress-free temp $T_{\sigma\text{-}free}$
		$\alpha_y - \alpha_x$	α_x*	α_y	
Glass	-0.00618	14.8	8.6	23.4	97
Carbon (Type2)	-0.00514	34.3	0.02	34.3	64

* Values from a textbook

Next, we will calculate the residual stress of the warped panel using the equations derived in Appendix B. The residual stress of the warped panel is a combination of the residual stress at the flat condition plus the stress due to the warp. Table 8 shows the residual stress calculated based on the warp measurements at low temperature. The stress in the 0° ply is along the fiber and that in the 90° ply is transverse to the fiber. Due to the symmetry, these stresses are equivalent to the longitudinal stress of the 90° ply and the transverse stress of the 0° ply, respectively.

Table 8 Residual stress in the warped condition

Material	Temp	Warp	Longitudinal stress in 0 [ksi]			Transverse stress in 90 [ksi]		
	[C]	[in]	top	average	middle	middle	average	bottom
Glass	23	0.46	1.5	-0.4	-2.2	0.7	0.4	0.1
	-14	0.69	2.3	-0.5	-3.3	1.0	0.5	0.1
	-78	0.86	2.8	-0.7	-4.1	**1.2**	0.7	0.1
Carbon (Type2)	23	0.21	3.1	-0.7	-4.4	0.9	0.7	0.5
	-14	0.40	5.9	-1.3	-8.4	1.7	1.3	0.9
	-78	0.51	7.4	-1.6	-10.6	**2.1**	1.6	1.1

The compressive and tensile strengths are much higher than the observed longitudinal stresses in the 0° ply, and therefore the 0° ply will not fail.

The bending test result of glass/polyester shown in Table 1 and 2 indicates that the transverse tensile strength of glass is Y=3.16ksi, which is higher than the measured transverse stress of 1.2ksi at −78°C. Cracks were observed in the glass panel at this temperature, which suggests that the surface stress exceeded the transverse tensile strength.

One effect that can contribute to the higher surface stress is the transient thermal effect due to the mismatch of the temperatures at the surface and within the laminate. The complex effect of transient thermal stress will not be addressed here, but we can calculate the first order effect using the results from Tables 2 and 7. When the panel was cooled down to −78°C using dry ice, it is reasonable to assume that the surface cooled down rapidly while the interior cooled down more gradually due to the low thermal conductivity in the thickness direction. Assuming a worst case where the laminate remains flat and unchanged at room temperature, while the local surface contracts completely at −78°C, the maximum residual stress can be approximated by

$$\sigma_{R,local} = -E_y \alpha_y \Delta T = 2718 psi = 2.72 ksi \qquad (5)$$

This stress is much higher than the residual stress at the warped condition and is close to the transverse tensile strength measured from the bending test. In reality, there will also be high level of shear stress involved, which was ignored here.

For the carbon/polyester (Type2), the transverse tensile strength is Y=4.24ksi from the bending test and Y=1.76ksi from the tension test. The transverse tensile stress at –78°C was 2.1ksi, which is less than the bending test result and higher than the tension test result. Cracks were not observed in the carbon panel, which either means that the actual transverse strength was higher than 2.1ksi, or that the microcracks were confined to the small region of high local stress and were not observed from the outside.

Assuming the same worst case as above, the residual stress at a local surface can reach

$$\sigma_{R,local} = -E_y \alpha_y \Delta T = 2632 psi = 2.63 ksi \qquad (6)$$

This stress is still below the transverse tensile strength measured from the bending test and above that from the tension test.

4. Bend-Twist Coupling Test

The purpose of the bend-twist coupling tests was to evaluate the predictability of the bend-twist analysis of the carbon and glass hybrid composite beam, based on the separately measured material properties of the carbon and glass composites. The analyses were performed both analytically and numerically using the commercial finite element analysis code ANSYS.

4.1 Test Configuration

The effect of the bend-twist coupling was measured using the special hybrid laminate with three layers of glass fibers in 0°, and three layers of carbon fibers in –30°. This layup is neither symmetric nor balanced, and the stretch, shear, bending, and twist are all coupled.

In the test, the loads were applied as concentrated loads at the tip or on a crossbeam attached to the tip of the beam. The concentrated load applied on this crossbeam can be considered as a combination of the vertical load P and torque T applied at the tip, as shown in Figure 5.

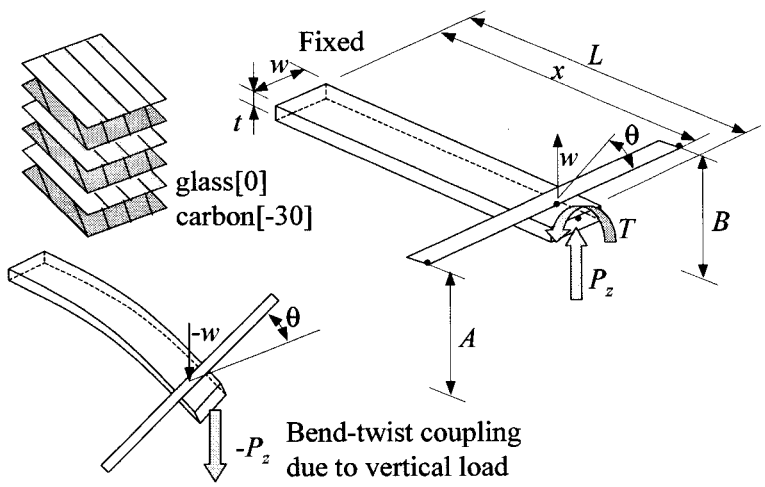

Figure 5 Bend-twist coupling test configuration

4.2 Test Results

The test results are shown in Tables 9 and 10. Table 9 shows the results from the test where only the downward (negative) tip load was applied and no torque. Note that the beam twists proportionally to the vertical deflection showing the bend-twist coupling.

The deflection in the table is the average value of the two measurements at both ends of the crossbeam. The twist is calculated from these two measurements by the following equation.

$$\theta = \frac{\Delta B - \Delta A}{l} \tag{7}$$

where ΔA is the change in the measurement A, ΔB is the change in B, and l is the length of the crossbeam.

Table 9 Bend-twist test results (Tip load only)

		Baseline	Tip Load Pz		
		Self Weight	Case1	Case2	Case3
Tip load	(lb)	0	-0.43	-0.88	-1.10
Torque	(lb-in)	0	0	0	0
A	(in)	12.9	12.1	11.2	10.8
B	(in)	11.0	9.6	7.9	7.1
ΔA	(in)	0.0	-0.9	-1.8	-2.2
ΔB	(in)	0.0	-1.4	-3.1	-3.9
deflection	(in)	0.0	-1.1	-2.4	-3.0
twist	(radian)	0.000	-0.021	-0.055	-0.070

Table 10 shows the results from the test where the tip was supported vertically. In this condition, the tip will experience a reaction force from the support. (See Appendix A for detailed test results.)

Table 10 Bend-twist test results (Supported at tip)

		Baseline	Torque
		Supported	Case4
Tip load	(lb)	0	0.092
Torque	(lb-in)	0	5.2
A	(in)	14.33	13.88
B	(in)	13.63	14.20
ΔA	(in)	0.00	-0.46
ΔB	(in)	0.00	0.57
deflection	(in)	0.00	0.06
twist	(radian)	0.000	0.043

4.3 Analysis

The bend-twist coupling of the $[0°_{glass}/-30°_{carbon}]$ laminate was calculated analytically from the material properties obtained by the bending and tension tests. The derivation of

the equations is shown in Appendix B. The sign convention used for the analytical calculation is shown in Figure 6.

To supplement the analysis, a finite element analysis was performed using the commercial code ANSYS. The material properties were the same as those used in the analytical calculation. Other hypothetical test configurations, such as the tension-twist coupling, were calculated analytically and numerically.

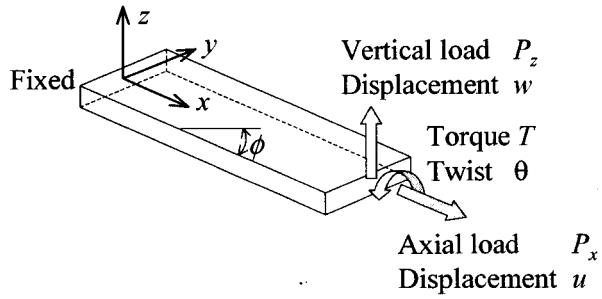

Figure 6 Sign convention for the applied loads and displacements

Table 11 shows the comparison of the analytical and numerical predictions and the test measurements. We observe good agreements between the analytical and numerical results and the test measurements.

Table 11 Bend-twist coupling calculation

	Tip Load			Torque	Theoretical		
	Case1	Case2	Case3	Case4	Case5	Case6	Case7
Tip load (lb)	-0.43	-0.88	-1.10	0.092	1	0	0
Torque (lb-in)	0	0	0	5.2	0	1	0
Axial load (lb)	0	0	0	0	0	0	1
Deflection (in)							
Test	-1.1	-2.4	-3.0	0.060	N/A	N/A	N/A
Analytical	-1.13	-2.28	-2.86	0.0078	2.62	-0.063	0.00098
FEM	-1.13	-2.28	-2.86	0.0064	2.57	-0.062	0.00096
Twist (10^{-3} radian)							
Test	-21	-55	-70	43	N/A	N/A	N/A
Analytical	-29.6	-59.9	-75.0	28.6	68.7	-7.16	0.0531
FEM	-29.5	-59.8	-75.0	34.2	67.2	-8.20	0.0532
Stretch (10^{-3} in)							
Test	N/A	N/A	N/A	N/A	N/A	N/A	N/A
Analytical	-0.46	-0.93	-1.16	0.145	1.07	-0.0531	0.0296
FEM	-0.45	-0.91	-1.14	0.148	1.05	-0.0532	0.0297

5. Conclusion

The material properties of the panel fabricated by the SCRIMP process were comparable to those from other low-cost composite manufacturing process. The carbon/polyester composite showed about twice the stiffness in the fiber direction compared to those of glass/polyester composites.

Another important finding is the significant level of residual stress although the panel was cured at room temperature. We suspect two sources of shrinkage that lead to this residual stress. One is the natural shrinkage of the resin during the cure process, which is independent of the curing temperature. Another source is the thermal expansion due to the elevated temperature caused by the exothermal condition during the cure, which is common in typical epoxy and polyester resins. In other words, although no additional heat was added, the resin heated up during the cure process and hardened at this elevated temperature. When the panel cooled down to room temperature, the resin contracted and contributed partly to the residual stress.

We have demonstrated how residual stress and stress-free temperature can be measured from the warping test of asymmetric panels. These values are valuable in the analysis and design of composite structures.

We were also able to demonstrate that the bend-twist coupling of the carbon and glass hybrid composite beam can be analyzed both numerically and analytically using the lamination theory. Analytical equations are more useful than the numerical results for the parameter study and design optimization of the hybrid composite structures. For wind turbine applications, we can design hybrid composite blades that have a built-in passive control of the blade pitch,

6. Acknowledgements

We would like to thank the Sandia National Laboratories for their support of this research, especially Dr. Paul Veers who has contributed to this report through his comments and insights. We would also like to thank the Air Force Research Laboratory Kirtland Air Force Base for the partial funding of our study of the residual stress and the effect of post-cure.

7. Reference

1. Tsai, Stephen W., *Theory of Composite Design*, 1992, Think Composites, Dayton.

Appendix A Detailed Test Results

Table A-1 Bending test results (Glass/Polyester)

Material	Direction	Post cure	Specimen	Width (in)	Thickness (in)	Span (in)	P/disp (lbf/in)	Failure Load (lbf)	Failure Mode	Modulus Ex	(msi)	Strength X'	(ksi)	Stress at Failure τ_{xy}	(ksi)
E-glass/ polyester	longitudinal bending	none	G-LT-2	0.490	0.150	4/2	1176	312	compression	5.69		84.9		3.22	
			G-LT-3	0.490	0.150	4/2	1167	320	compression	5.65		87.1		3.27	
			G-LT-4	0.492	0.150	4/2	1160	328	compression	5.59	average	88.9	average	3.33	average
			G-LT-5	0.489	0.150	4/2	1141	309	compression	5.53	5.62	84.3	86.3	3.16	3.25
		60Cx8hrs	PG-LT-1	0.489	0.150	4/2	1070	313	compression	5.19		85.3		3.20	
			PG-LT-2	0.486	0.150	4/2	1180	338	compression	5.76	average	92.7	average	3.48	average
			PG-LT-3	0.488	0.150	4/2	1190	331	compression	5.78	5.58	90.4	89.5	3.39	3.36

Material	Direction	Post cure	Specimen	Width (in)	Thickness (in)	Span (in)	P/disp (lbf/in)	Failure Load (lbf)	Failure Mode	Modulus Ey	(msi)	Strength Y	(ksi)
E-glass/ polyester	transverse bending	none	G-TT-1	0.484	0.150	4/2	239	12.0	tension	1.17		3.29	
			G-TT-2	0.490	0.150	4/2	251	12.8	tension	1.23		3.54	
			G-TT-3	0.490	0.150	4/2	229	11.2	tension	1.14		3.12	
			G-TT-4	0.492	0.150	4/2	207	9.6	tension	1.00	average	2.60	average
			G-TT-5	0.489	0.150	4/2	239	11.6	tension	1.19	1.15	3.25	3.16
		60Cx8hrs	PG-TT-1	0.489	0.150	4/2	286	12.6	tension	1.40		3.46	
			PG-TT-2	0.486	0.150	4/2	290	12.2	tension	1.43	average	3.39	average
			PG-TT-3	0.488	0.150	4/2	268	11.6	tension	1.33	2.81	3.23	4.15

Table A-2 Bending test results (Carbon/Polyester Type1)

Material	Direction	Post cure	Specimen	Width (in)	Thickness (in)	Span (in)	P/disp (lbf/in)	Failure Load (lbf)	Failure Mode	Modulus Ex	(msi)	Strength S	(ksi)	Stress at Failure σ_x	(ksi)
carbon/ polyester	longitudinal bending	none	C-LT-1	0.482	0.222	4/2	6946	733	interlaminar shear	10.5		5.14		92.6	
		60Cx8hrs	PC-LT-1	0.495	0.220	4/2	7494	843	interlaminar shear	11.4		5.81		105.6	

Material	Direction	Post cure	Specimen	Width (in)	Thickness (in)	Span (in)	P/disp (lbf/in)	Failure Load (lbf)	Failure Mode	Modulus Ey	(msi)	Strength Y	(ksi)
carbon/ polyester (Type1)	transverse bending	none	G-TT-1	0.490	0.220	4/2	528	35.2	tension	0.79		4.37	
			G-TT-4	0.494	0.220	4/2	477	32.6	tension	0.71	average	4.02	average
			G-TT-5	0.493	0.220	4/2	508	36.4	tension	0.75	0.75	4.49	4.29
		60Cx8hrs	PG-TT-1	0.490	0.220	4/2	599	31.0	tension	0.92		3.92	
			PG-TT-2	0.485	0.220	4/2	573	31.2	tension	0.89	average	3.99	average
			PG-TT-3	0.492	0.220	4/2	542	30.0	tension	0.83	4.38	3.78	3.79

Table A-3 Bending test results (Carbon/Polyester Type2)

Material	Direction	Post cure	Specimen	Width (in)	Thickness (in)	Span (in)	P/disp (lbf/in)	Failure Load (lbf)	Failure Mode	Modulus Ex	(msi)	Strength S	(ksi)	Stress at Failure σ_x	(ksi)
carbon/ polyester (Type2)	longitudinal bending	none	LB-1	0.488	0.299	4/2	12632	518	interlaminar shear	7.75		2.66		35.6	
			LB-2	0.497	0.300	4/2	14438	753	interlaminar shear	8.61		3.79		50.5	
			LB-3	0.485	0.294	4/2	14858	682	interlaminar shear	9.64		3.59		48.8	
			LB-4	0.497	0.298	4/2	14452	731	interlaminar shear	8.79	average	3.70	average	49.7	average
			LB-5	0.491	0.290	4/2	13616	531	interlaminar shear	8.28	8.61	2.69	3.29	36.1	44.1

Material	Direction tension	Post cure	Specimen	Width (in)	Thickness (in)	Length (in)	P/disp (lbf/in)	Failure Load (lbf)	Failure Mode	Modulus Ey	(msi)	Strength Y	(ksi)
carbon/ polyester (Type2)	transverse bending	none	TB-1	0.454	0.292	4/2	1232	-58.0	tension	0.87		4.49	
			TB-2	0.461	0.296	4/2	1147	-57.4	tension	0.77		4.26	
			TB-3	0.480	0.297	4/2	1076	-61.4	tension	0.68		4.35	
			TB-4	0.489	0.292	4/2	1170	-56.6	tension	0.77	average	4.07	average
			TB-5	0.490	0.294	4/2	1110	-56.8	tension	0.71	0.76	4.02	4.24

Table A-4 Tension test results (Carbon/Polyester Type2)

Material	Direction tension	Post cure	Specimen	Width (in)	Thickness (in)	Length (in)	P/disp (lbf/in)	Failure Load (lbf)	Failure Mode	Modulus Ex	(msi)	Strength X	(ksi)
carbon/ polyester (Type2)	longitudinal tension	none	LT-1	0.476	0.280			5946	premature	11.80		>44.6	
			LT-2	0.474	0.281			5078	premature	12.00		>38.1	
			LT-3	0.486	0.287			N/A	N/A	12.49			
			LT-4	0.483	0.290			N/A	N/A	12.96			
			LT-5	0.470	0.301			N/A	N/A	13.58	12.57		

Material	Direction tension	Post cure	Specimen	Width (in)	Thickness (in)	Length (in)	P/disp (lbf/in)	Failure Load (lbf)	Failure Mode	Modulus Ey	(msi)	Strength Y	(ksi)
carbon/ polyester (Type2)	transverse tension	none	TT-1	0.985	0.289			523	tension	0.925		1.85	
			TT-2	0.981	0.290			494	tension			1.74	
			TT-3	0.995	0.286			511	tension			1.80	
			TT-4	0.988	0.287			501	tension			1.77	
			TT-5	0.985	0.291			493	tension			1.72	average
			TT-6	0.995	0.287			485	tension			1.70	1.76

Table A-5 Plate warping test results (Post-cure effect)

Specimen	Post Cure	Measured at	Measurements (in)								Average	Res Stress
glass [0/90] -1	none	RT, Dry	0.32	0.33	0.30	0.33	0.32	0.30	0.24	0.24	0.30	0.62
	60Cx.5hrs	RT, Dry	0.46	0.46	0.41	0.43	0.44	0.43	0.43	0.41	0.43	0.91
	+ 80Cx.5hrs	RT, Dry	0.57	0.57	0.51	0.55	0.61	0.69	0.64	0.64	0.59	1.25
	+ 80Cx.5hrs	RT, Dry	0.82	0.82	0.82	0.85	0.73	0.70	0.77	0.75	0.78	1.64
	+ 100Cx.5hrs	RT, Dry	0.83	0.81	0.87	0.88	0.82	0.81	0.74	0.74	0.81	1.70
glass [0/90] -2	none	RT, Dry	0.42	0.42	0.40	0.39	0.24	0.25	0.28	0.27	0.33	0.70
	60Cx4hrs	RT, Dry	0.57	0.57	0.58	0.57	0.58	0.56	0.57	0.55	0.57	1.19
	60Cx8hrs	RT, Dry	0.60	0.59	0.62	0.60	0.67	0.64	0.71	0.70	0.64	1.35
	Soak	RT, Wet									0.49	1.03

Soaked at 60C for 100 hours, weight gain of 2.5%

Specimen	Post Cure	Measured at	Measurements (in)								Average	Res Stress
carbon [0/90] -2 (Type1)	none	RT, Dry	0.13	0.16	0.16	0.17	0.17	0.17	0.16	0.13	0.15	0.55
	60Cx4hrs	RT, Dry	0.36	0.35	0.31	0.31	0.36	0.36	0.32	0.29	0.33	1.17
	60Cx8hrs	RT, Dry	0.42	0.42	0.41	0.39	0.37	0.36	0.41	0.38	0.40	1.39
	Soak	RT, Wet									0.36	1.25

Soaked at 60C for 100 hours, weight gain of 0.28%

Table A-6 Plate warping test results (High temperature)

Specimen	Post Cure	Measured at	Measurements (in)				Calculations		
			w_1	w_2	w_3	w_4	ΔT	Δw_1	$w/\Delta T$
glass [0/90] -1	none	RT, Dry	0.320	0.334	0.302	0.325			
	60Cx.5hrs	60C	0.265	0.340	0.280	0.316	37	0.199	0.0054
		RT, Dry	0.464	0.464	0.410	0.426			
	60+80Cx.5hr	80C	0.173	0.210	0.275	0.202	57	0.393	0.0069
		RT, Dry	0.566	0.567	0.509	0.548			
	60+80Cx1hr	80C	0.468	0.496	0.550	0.633	57	0.347	0.0061
		RT, Dry	0.815	0.815	0.817	0.845			
	60,80+	100C	0.305	0.370			77	0.525	0.0068
	100Cx.5hrs	RT, Dry	0.830	0.809	0.869	0.884			

Table A-7 Plate Warping test results (Low temperature)

Specimen	Post Cure	Measured at	Average measurements (in)	Residual Stress (ksi)
glass [0/90] -3	none	23	0.48	1.01
	none	-14	0.69	1.45
	none	-78	0.87	1.83
glass [0/90] -4	none	23	0.44	0.92
	none	-14		
	none	-78	0.84	1.76

Specimen	Post Cure	Measured at	Average measurements (in)	Residual Stress (ksi)
carbon [0/90] -1 (Type2)	none	23	0.21	1.16
	none	-14	0.40	2.21
	none	-78	0.49	2.71
carbon [0/90] -2 (Type2)	none	23	0.21	1.16
	none	-14		
	none	-78	0.52	2.88

Table A-8 Beam bend-twist coupling test results

		Baseline	Tip Load		
		Self Weight	Case1	Case2	Case3
Tip load	(lb)	0	0.43	0.88	1.10
Torque	(lb-in)	0	0	0	0
A	(in)	12.94	12.06	11.19	10.75
B	(in)	11.00	9.63	7.94	7.13
ΔA	(in)	0.00	-0.88	-1.75	-2.19
ΔB	(in)	0.00	-1.38	-3.06	-3.88
deflection	(in)	0.00	-1.13	-2.41	-3.03
twist	(radian)	0.000	-0.021	-0.055	-0.070

		Baseline	Torque
		Self Weight	Case4
Tip load	(lb)	0	-0.09
Torque	(lb-in)	0	5.16
A	(in)	14.33	13.88
B	(in)	13.63	14.20
ΔA	(in)	0.00	-0.46
ΔB	(in)	0.00	0.57
deflection	(in)	0.00	0.06
twist	(radian)	0.000	0.043

Appendix B Analytical Calculation

1. Lamination Theory

In the lamination theory, the strains are defined as functions of the mid-plane strains ε^0 and the curvature κ:

$$\vec{\varepsilon} = \begin{Bmatrix} \varepsilon_1^0 + \kappa_1 z \\ \varepsilon_2^0 + \kappa_2 z \\ \varepsilon_6^0 + \kappa_6 z \end{Bmatrix} \tag{B1}$$

The mid-plane strains and curvature of a composite laminate under given load and moment can be calculated by the following matrix equation.

$$\begin{Bmatrix} \vec{N} \\ \vec{M} \end{Bmatrix} = \begin{pmatrix} A & B \\ B & D \end{pmatrix} \begin{Bmatrix} \vec{\varepsilon^0} \\ \vec{\kappa} \end{Bmatrix} \tag{B2}$$

or in inverse form,

$$\begin{Bmatrix} \vec{\varepsilon^0} \\ \vec{\kappa} \end{Bmatrix} = \begin{pmatrix} a & b \\ b & d \end{pmatrix} \begin{Bmatrix} \vec{N} \\ \vec{M} \end{Bmatrix} = \begin{pmatrix} A & B \\ B & D \end{pmatrix}^{-1} \begin{Bmatrix} \vec{N} \\ \vec{M} \end{Bmatrix} \tag{B3}$$

where N is the applied load per unit width and M is the applied moment per unit width. The A, B, and D matrices are calculated from the components of the ply stiffness matrix.

$$\begin{aligned} A_{jk}^i &= \sum_{i=1}^{n} Q_{jk}^i (h_i - h_{i-1}) \\ B_{jk}^i &= \sum_{i=1}^{n} Q_{jk}^i \frac{h_i^2 - h_{i-1}^2}{2} \\ D_{jk}^i &= \sum_{i=1}^{n} Q_{jk}^i \frac{h_i^3 - h_{i-1}^3}{3} \end{aligned} \tag{B4}$$

The mid-plane strains and curvatures can be related to the displacements with the following equations.

$$\vec{\varepsilon^0} = \begin{Bmatrix} \varepsilon_1^0 \\ \varepsilon_2^0 \\ \varepsilon_6^0 \end{Bmatrix} = \begin{Bmatrix} \dfrac{\partial u}{\partial x} \\ \dfrac{\partial v}{\partial y} \\ \dfrac{\partial v}{\partial x} + \dfrac{\partial u}{\partial y} \end{Bmatrix} \tag{B5}$$

$$\vec{\kappa} = \begin{Bmatrix} \kappa_1 \\ \kappa_2 \\ \kappa_6 \end{Bmatrix} = \begin{Bmatrix} -\dfrac{\partial^2 w}{\partial x^2} \\ -\dfrac{\partial^2 w}{\partial y^2} \\ -2\dfrac{\partial^2 w}{\partial x \partial y} \end{Bmatrix} \tag{B6}$$

where x-axis is along the length, y–axis is along the width, and z–axis is along the thickness. Similarly, the displacements u, v, and w are along the x, y, and z axes, respectively.

2. Warping due to the Thermal Expansion

In the warping test of a square plate, no external loads N or M are applied, and the warping is due solely to the difference in the thermal expansion in the 0° and 90° directions. The curvatures can be measured easily from the warp. The mid-plane strains are hard to measure but also exist. We will use the indices x and y to represent the 0° and 90° directions, respectively.

The thermal strains are a function of the temperature difference ΔT, and the coefficients of thermal expansion (CTE) α_x and α_y.

$$\begin{aligned} \varepsilon_{x,T}^0 &= \alpha_x \Delta T \\ \varepsilon_{y,T}^0 &= \alpha_y \Delta T \end{aligned} \tag{B7}$$

In unconstrained condition, the plies will expand freely with no stresses. In the case of a laminate with plies in two or more directions, the expansions of the plies are constrained by each other, which leads to the residual stresses in the plies. If a laminate is not symmetric, these residual stresses can make the laminate warp. A symmetric laminate will not warp, but will experience higher residual stresses.

Let us calculate the residual stress of a square $[0_n/90_n]$ asymmetric laminate. First, let us assume that the laminate is constrained such that it will not warp. The thermal strains apply only to the normal strains and thus we have the following relations between the thermal strains ε_T and the residual strains ε_R.

$$\begin{aligned}
\varepsilon_x^0 &= \varepsilon_{x,T}^0 + \varepsilon_{x,R}^0 \\
\varepsilon_y^0 &= \varepsilon_{y,T}^0 + \varepsilon_{y,R}^0 \\
\varepsilon_{xy}^0 &= 0 \\
\kappa_x &= \kappa_y = \kappa_{xy} = 0
\end{aligned} \tag{B8}$$

The residual strains will create the following residual stresses

$$\begin{aligned}
\sigma_{x,R} &= Q_{xx}\varepsilon_{x,R}^0 + Q_{xy}\varepsilon_{y,R}^0 \\
\sigma_{y,R} &= Q_{xy}\varepsilon_{x,R}^0 + Q_{yy}\varepsilon_{y,R}^0
\end{aligned} \tag{B9}$$

The total mid-plane strains in the 0° and 90° directions are equal since the plate is constrained from warping. Also, the residual stresses are equal and opposite from the equilibrium. Therefore,

$$\begin{aligned}
\varepsilon_x^0 &= \varepsilon_y^0 \equiv \varepsilon^0 \\
\sigma_{x,R} &= -\sigma_{y,R} \equiv \sigma_R
\end{aligned} \tag{B10}$$

Solve these two equations to obtain

$$\begin{aligned}
\varepsilon_{x,R}^0 &= \frac{Q_{yy} + Q_{xy}}{Q_{xx} + 2Q_{xy} + Q_{yy}}(\alpha_y - \alpha_x)\Delta T \\
\varepsilon_{y,R}^0 &= -\frac{Q_{xx} + Q_{xy}}{Q_{xx} + 2Q_{xy} + Q_{yy}}(\alpha_y - \alpha_x)\Delta T
\end{aligned} \tag{B11}$$

$$\sigma_R = \frac{Q_{xx}Q_{yy} - Q_{xy}^2}{Q_{xx} + 2Q_{xy} + Q_{yy}}(\alpha_y - \alpha_x)\Delta T \tag{B12}$$

These equations are also true for any symmetric cross ply laminate with equal numbers of 0° and 90° plies. Typically, CTE of unidirectional laminates in the transverse direction, α_y, is larger than that in the fiber direction, α_x, and thus the residual stresses are positive in the 0° plies and negative in the 90° plies.

In the case of an asymmetric laminate, the moments required to keep this laminate flat are,

$$\begin{aligned}
M_1 &= -\sigma_{x,R}\int_0^{t/2} z\,dz - \sigma_{y,R}\int_{t/2}^{0} z\,dz = -\frac{t^2}{4}\sigma_R \equiv M \\
M_2 &= -M
\end{aligned} \tag{B13}$$

Apply these moments to Equation (B3) to calculate the mechanical normal strains ε^{0}_{M} and curvatures κ_M.

$$\begin{Bmatrix} \varepsilon^0_{1,M} \\ \varepsilon^0_{2,M} \\ \varepsilon^0_{6,M} \\ \kappa_{1,M} \\ \kappa_{2,M} \\ \kappa_{6,M} \end{Bmatrix} = \begin{pmatrix} a_{11} & a_{12} & 0 & b_{11} & 0 & 0 \\ a_{12} & a_{11} & 0 & 0 & -b_{11} & 0 \\ 0 & 0 & a_{11} & 0 & 0 & 0 \\ b_{11} & 0 & 0 & d_{11} & d_{12} & 0 \\ 0 & -b_{11} & 0 & d_{12} & d_{11} & 0 \\ 0 & 0 & 0 & 0 & 0 & d_{66} \end{pmatrix} \begin{Bmatrix} 0 \\ 0 \\ 0 \\ M \\ -M \\ 0 \end{Bmatrix}$$

$$\varepsilon^0_M \equiv \varepsilon^0_{1,M} = \varepsilon^0_{2,M} = b_{11}M$$

$$\varepsilon^0_{6,M} = 0 \qquad \text{(B14)}$$

$$\kappa_M \equiv \kappa_{1,M} = -\kappa_{2,M} = (d_{11} - d_{12})M$$

$$\kappa_{6,M} = 0$$

Note that the 6×6 stiffness matrix for the [0°$_n$/90°$_n$] laminate has many zero and common components.

In the warping test, the amount of warp was measured as the deflection of the two corners of the plate when the other two corners were fixed. Using Equation (B6) the deflection w and the curvature κ can be related by the following equation.

$$w = -\kappa L^2 / 2 \qquad \text{(B15)}$$

where L is the length and the width of the square plate.

The residual stresses at this warped condition can be calculated considering only the residual and mechanical strains.

$$\begin{aligned} \sigma_{1,R}(z) &= Q_{11}\left(\varepsilon^0_{1,R} + \varepsilon^0_M + \kappa_M z\right) + Q_{12}\left(\varepsilon^0_{2,R} + \varepsilon^0_M - \kappa_M z\right) \\ &= \begin{cases} Q_{xx}\left(\varepsilon^0_{x,R} + \varepsilon^0_M + \kappa_M z\right) + Q_{xy}\left(\varepsilon^0_{y,R} + \varepsilon^0_M - \kappa_M z\right) & (0 \le z \le t/2) \\ Q_{yy}\left(\varepsilon^0_{y,R} + \varepsilon^0_M + \kappa_M z\right) + Q_{xy}\left(\varepsilon^0_{x,R} + \varepsilon^0_M - \kappa_M z\right) & (-t/2 \le z \le 0) \end{cases} \\ &= \begin{cases} \sigma_R + \left(Q_{xx} + Q_{xy}\right)\varepsilon^0_M + \left(Q_{xx} - Q_{xy}\right)\kappa_M z & (0 \le z \le t/2) \\ -\sigma_R + \left(Q_{yy} + Q_{xy}\right)\varepsilon^0_M + \left(Q_{yy} - Q_{xy}\right)\kappa_M z & (-t/2 \le z \le 0) \end{cases} \end{aligned} \qquad \text{(B16)}$$

Similarly,

$$\sigma_{2,R}(z) = \begin{cases} -\sigma_R + \left(Q_{yy} + Q_{xy}\right)\varepsilon^0_M - \left(Q_{yy} - Q_{xy}\right)\kappa_m z & (0 \le z \le t/2) \\ \sigma_R + \left(Q_{xx} + Q_{xy}\right)\varepsilon^0_M - \left(Q_{xx} - Q_{xy}\right)\kappa_m z & (-t/2 \le z \le 0) \end{cases} \qquad \text{(B18)}$$

3. Bend-Twist Coupling of Unbalanced Laminate

In this section, we will demonstrate how we can calculate the deflections and the twist of a hybrid composite beam. The loads that were considered here are axial load P_x, concentrated vertical load at the tip P_z, and the torque T. These loads are converted to loads per unit width with the following equations.

$$\begin{aligned} N_1 &= P_x / b \\ P &= P_z / b \\ M_6 &= -T / 2b \end{aligned} \tag{B19}$$

The reason for the factor of two in the last equation is not trivial, but is due to the difference in the definition of the torque T and twisting moment M_6. The torque is applied on one edge, and the opposite edge experiences an equal and opposite torque as a reaction. On the other hand, the twisting moment is defined as the moment applied on four edges of the plate, which effectively becomes half of the torque.

The applied loads N_1 and M_6 are constant along the length, but the constant load P create axial bending moment that is a function of the location x.

$$M_1(x) = P(x - L) \tag{B20}$$

The mid-plane strains and curvatures due to the combinations of N_1, M_1, and M_6 can be calculated using Equation (B3).

$$\begin{Bmatrix} \varepsilon_1^0 \\ \varepsilon_{2,}^0 \\ \varepsilon_6^0 \\ \kappa_1 \\ \kappa_2 \\ \kappa_6 \end{Bmatrix} = \begin{pmatrix} a_{11} & a_{12} & a_{16} & b_{11} & b_{12} & b_{16} \\ a_{12} & a_{22} & a_{26} & b_{12} & b_{22} & b_{26} \\ a_{16} & a_{26} & a_{66} & b_{16} & b_{26} & b_{66} \\ b_{11} & b_{12} & b_{16} & d_{11} & d_{12} & d_{16} \\ b_{12} & b_{22} & b_{26} & d_{12} & d_{22} & d_{26} \\ b_{16} & b_{26} & b_{66} & d_{16} & d_{26} & d_{66} \end{pmatrix} \begin{Bmatrix} N_1 \\ 0 \\ 0 \\ M_1 \\ 0 \\ M_6 \end{Bmatrix}$$

$$\begin{aligned} \varepsilon_1^0 &= a_{11}N_1 + b_{11}M_1 + b_{16}M_6 \\ \kappa_1^0 &= b_{11}N_1 + d_{11}M_1 + d_{16}M_6 \\ \kappa_1^0 &= b_{16}N_1 + d_{16}M_1 + d_{66}M_6 \\ \varepsilon_2^0 &= \varepsilon_6^0 = \kappa_1^0 = 0 \end{aligned} \tag{B21}$$

Note that the 6×6 stiffness matrix is fully populated since this laminate is neither symmetric or balanced.

These mid-plane strains and curvatures are related to the deflections by Equations (B5) and (B6). By integrating these values with appropriate boundary conditions, we can

calculate the deflection and the twist of the composite beam. In the case of the cantilever test, the boundary conditions are the following.

$$\begin{aligned} &\text{vertical displacement}: w(0) = 0 \\ &\text{vertical slope}: \quad w'(0) = 0 \\ &\text{axial displacement}: \quad u(0) = 0 \\ &\text{twist}: \quad \theta(0) = 0 \end{aligned} \tag{B22}$$

Axial deflection due to the axial load per width N_1, concentrated load per width P, and twisting moment per width M_6 are,

$$\begin{aligned} u_N(x) &= a_{11} N_1 x \\ u_p(x) &= b_{11} P\left(x^2/2 - Lx\right) \\ u_M(x) &= b_{16} M_6 x \end{aligned} \tag{B23}$$

Vertical deflection due to the same loads per width N_1, P and M_6 are,

$$\begin{aligned} w_N(x) &= -b_{11} N_1 x^2/2 \\ w_p(x) &= -d_{11} P\left(x^3/6 - Lx^2/2\right) \\ w_M(x) &= -d_{16} M_6 x^2/2 \end{aligned} \tag{B24}$$

Twist due to the same loads per width N_1, P and M_6 are,

$$\begin{aligned} \theta_N(x) &= -b_{16} N_1 x/2 \\ \theta_p(x) &= -d_{16} P(x^2/4 - Lx/2) \\ \theta_M(x) &= -d_{66} M_6 x/2 \end{aligned} \tag{B25}$$

DISTRIBUTION

H. Ashley
Dept. of Aeronautics and
Astronautics Mechanical Engr.
Stanford University
Stanford, CA 94305

K. Bergey
University of Oklahoma
Aero Engineering Department
Norman, OK 73069

D. Berry
TPI Composites Inc.
373 Market Street
Warren, RI 02885

R. Blakemore
GE Wind
13681 Chantico Road
Tehachapi, CA 93561

C. P. Butterfield
NREL
1617 Cole Boulevard
Golden, CO 80401

G. Bywaters
Northern Power Systems
Box 999
Waitsfield,VT 05673

J. Cadogan
Office of Wind and Hydro Technology
EE-12
U.S. Department of Energy
1000 Independence Avenue SW
Washington, DC 20585

D. Cairns
Montana State University
Mechanical & Industrial Engineering Dept.
220 Roberts Hall
Bozeman, MT 59717

S. Calvert
Office of Wind and Hydro Technology
EE-12
U.S. Department of Energy
1000 Independence Avenue SW
Washington, DC 20585

J. Chapman
OEM Development Corp.
840 Summer St.
Boston, MA 02127-1533

Kip Cheney
PO Box 456
Middlebury, CT 06762

C. Christensen, Vice President
GE Wind
13681 Chantico Road
Tehachapi, CA 93561

R. N. Clark
USDA
Agricultural Research Service
P.O. Drawer 10
Bushland, TX 79012

C. Cohee
Foam Matrix, Inc.
1123 East Redondo Blvd.
Inglewood, CA 90302

J. Cohen
Princeton Economic Research, Inc.
1700 Rockville Pike
Suite 550
Rockville, MD 20852

C. Coleman
Northern Power Systems
Box 999
Waitsfield, VT 05673

K. J. Deering
The Wind Turbine Company
1261 120th Ave. NE
Bellevue, WA 98005

A. J. Eggers, Jr.
RANN, Inc.
744 San Antonio Road, Ste. 26
Palo Alto, CA 94303

D. M. Eggleston
DME Engineering
1605 W. Tennessee Ave.
Midland, TX 79701-6083

P. R. Goldman
Director
Office of Wind and Hydro Technology
EE-12
U.S. Department of Energy
1000 Independence Avenue SW
Washington, DC 20585

D. Griffin
GEC
5729 Lakeview Drive NE, Ste. 100
Kirkland, WA 98033

C. Hansen
Windward Engineering
4661 Holly Lane
Salt Lake City, UT 84117

C. Hedley
Headwaters Composites, Inc.
PO Box 1073
Three Forks, MT 59752

D. Hodges
Georgia Institute of Technology
270 Ferst Drive
Atlanta, GA 30332

Bill Holley
3731 Oakbrook
Pleasanton, CA 94588

K. Jackson
Dynamic Design
123 C Street
Davis, CA 95616

E. Jacobsen
GE Wind
13000 Jameson Rd.
Tehachapi, CA 93561

G. James
Structures & Dynamics Branch, Mail Code ES2
NASA Johnson Space Center
2101 NASA Rd 1
Houston, TX 77058

M. Kramer
Foam Matrix, Inc.
PO Box 6394
Malibu CA 90264

A. Laxson
NREL
1617 Cole Boulevard
Golden, CO 80401

S. Lockard
TPI Composites Inc.
373 Market Street
Warren, RI 02885

J. Locke, Associate Professor
Wichita State University
207 Wallace Hall, Box 44
Wichita, KS 67620-0044

D. Malcolm
GEC
5729 Lakeview Drive NE, Ste. 100
Kirkland, WA 98033

J. F. Mandell
Montana State University
302 Cableigh Hall
Bozeman, MT 59717

T. McCoy
GEC
5729 Lakeview Drive NE, Ste. 100
Kirkland, WA 98033

L. McKittrick
Montana State University
Mechanical & Industrial Engineering Dept.
220 Roberts Hall
Bozeman, MT 59717

P. Migliore
NREL
1617 Cole Boulevard
Golden, CO 80401

A. Mikhail
Clipper Windpower Technology, Inc.
7985 Armas Canyon Road
Goleta, CA 93117

W. Musial
NREL
1617 Cole Boulevard
Golden, CO 80401

NWTC Library (5)
NREL
1617 Cole Boulevard
Golden, CO 80401

B. Neal
USDA
Agricultural Research Service
P.O. Drawer 10
Bushland, TX 79012

V. Nelson
Department of Physics
West Texas State University
P.O. Box 248
Canyon, TX 79016

T. Olsen
Tim Olsen Consulting
1428 S. Humboldt St.
Denver, CO 80210

R. Z. Poore
Global Energy Concepts, Inc.
5729 Lakeview Drive NE
Suite 100
Kirkland, WA 98033

R. G. Rajagopalan
Aerospace Engineering Department
Iowa State University
404 Town Engineering Bldg.
Ames, IA 50011

J. Richmond
MDEC
3368 Mountain Trail Ave.
Newbury Park, CA 91320

Michael Robinson
NREL
1617 Cole Boulevard
Golden, CO 80401

D. Sanchez
U.S. Dept. of Energy
Albuquerque Operations Office
P.O. Box 5400
Albuquerque, NM 87185

R. Sherwin
Atlantic Orient
PO Box 1097
Norwich, VT 05055

Brian Smith
NREL
1617 Cole Boulevard
Golden, CO 80401

J. Sommer
Molded Fiber Glass Companies/West
9400 Holly Road
Adelanto, CA 93201

K. Starcher
AEI
West Texas State University
P.O. Box 248
Canyon, TX 79016

A. Swift
University of Texas at El Paso
320 Kent Ave.
El Paso, TX 79922

J. Thompson
ATK Composite Structures
PO Box 160433
MS YC14
Clearfield, UT 84016-0433

R. W. Thresher
NREL
1617 Cole Boulevard
Golden, CO 80401

S. Tsai (5)
Stanford University
Aeronautics & Astronautics
Durand Bldg. Room 381
Stanford, CA 94305-4035

W. A. Vachon
W. A. Vachon & Associates
P.O. Box 149
Manchester, MA 01944

C. P. van Dam
Dept of Mech and Aero Eng.
University of California, Davis
One Shields Avenue
Davis, CA 95616-5294

B. Vick
USDA, Agricultural Research Service
P.O. Drawer 10
Bushland, TX 79012

K. Wetzel
K. Wetzel & Co., Inc.
PO Box 4153
4108 Spring Hill Drive
Lawrence, KS 66046-1153

R. E. Wilson
Mechanical Engineering Dept.
Oregon State University
Corvallis, OR 97331

M. Zuteck
MDZ Consulting
601 Clear Lake Road
Clear Lake Shores, TX 77565

M.S. 0557	T. J. Baca, 9125
M.S. 0557	T. G. Carne, 9124
M.S. 0708	H. M. Dodd, 6214 (25)
M.S. 0708	T. D. Ashwill, 6214 (10)
M.S. 0708	D. E. Berg, 6214
M.S. 0708	R. R. Hill, 6214
M.S. 0708	P. L. Jones 6214
M.S. 0708	D. L. Laird, 6214
M.S. 0708	D. W. Lobitz, 6214
M.S. 0708	M. A. Rumsey, 6214
M.S. 0708	H. J. Sutherland, 6214
M.S. 0708	P. S. Veers, 6214
M.S. 0708	J. Zayas, 6214
M.S. 0847	K. E. Metzinger, 9126
M.S. 0958	M. Donnelly, 14172
M.S. 1490	A. M. Lucero, 12660
M.S. 0612	Review & Approval Desk, 9612 For DOE/OSTI
M.S. 0899	Technical Library, 9616 (2)
M.S. 9018	Central Technical Files, 8945-1